Mechanical modeling of dowel action and the influence of small amounts of shear reinforcement on the shear-transfer actions in RC beams

Autrup, Frederik; Jørgensen, Henrik Brøner; Ruiz, Miguel Fernández; Hoang, Linh Cao

Published in:
Structural Concrete

Link to article, DOI:
10.1002/suco.202300082

Publication date:
2023

Document Version
Publisher's PDF, also known as Version of record

Received: 2 February 2023 | Revised: 24 April 2023 | Accepted: 3 May 2023

DOI: 10.1002/suco.202300082

ARTICLE

fib CEB-FIP WILEY

Mechanical modeling of dowel action and the influence of small amounts of shear reinforcement on the shear-transfer actions in RC beams

Frederik Autrup[1,2] | **Henrik Brøner Jørgensen**[2] | **Miguel Fernández Ruiz**[3] | **Linh Cao Hoang**[4]

[1]Department of Monitoring and Analyses of Existing Structures, Rambøll Denmark A/S, Copenhagen, Denmark

[2]Department of Technology and Innovation, University of Southern Denmark, Odense, Denmark

[3]Escuela Técnica Superior de Ingenieros de Caminos, Canales y Puertos, Universidad Politécnica de Madrid, Madrid, Spain

[4]Department of Civil and Mechanical Engineering, Technical University of Denmark, Kgs. Lyngby, Denmark

Correspondence
Frederik Autrup, Department of Monitoring and Analyses of Existing Structures, Rambøll Denmark A/S, Copenhagen, Denmark.
Email: fau@ramboll.dk

Funding information
Rambøll Fonden

Abstract

Dowel action of the longitudinal reinforcement in RC beams without and with small amounts of shear reinforcement is typically considered a constant shear contribution determined from the splitting strength of the concrete cover. However, in a recent experimental investigation by the authors, it was shown that the shear force transferred by dowel action for beams without shear reinforcement should be determined from the dowel displacement and a linear elastic model and a rigid plastic dowel model. This article is aimed at extending this model to also cover members with small amounts of shear reinforcement. To that aim, a novel approach to calculate the shear force carried by dowel action of the longitudinal reinforcement in both beams with and without shear reinforcement is presented. The model is derived by establishing an equilibrium of work between the internal stored elastic or dissipated plastic energy and the external work performed by the shear force in the dowel. Additionally, a method to determine the displacement of the dowel from DIC measurements is presented. For the remaining shear-transfer actions, reasonable constitutive models from the literature are adapted. On the basis of DIC measurements, the shear force carried by each of the shear-transfer actions is calculated for 16 shear tests of beams without and with small amounts of shear reinforcement. The sum of shear force carried by each of the shear-transfer actions is shown to predict the applied shear force fairly well, from the development of the critical shear crack until failure. Additionally, it is shown that for beams with shear reinforcement below the minimum requirements according to the current design standards, the shear capacity is governed by aggregate interlock, residual tensile stresses, and the inclination of the compression chord. While for beams with shear reinforcement above the minimum requirements, the shear capacity is governed by the shear reinforcement and dowel action.

KEYWORDS

dowel action, experimental investigation, linear elastic modeling, mechanical modeling, reinforced concrete, rigid plastic modeling, shear, shear-transfer actions

1 | INTRODUCTION

For existing concrete structures, such as highway bridges, the calculated load-bearing capacity is often a governing factor when assessing their service lifetime. In many cases, the assessment of the load-bearing capacity is performed on the basis of design models. Such models are, however, developed to cover a large variety of cases and may hinder an accurate assessment of the load-bearing capacity.[1] Within this frame, developing accurate models for the load-bearing capacity is a need to suitably evaluate the level of safety of the existing infrastructures and to avoid unnecessary strengthening and its associated environmental impact. Many of these highway bridges were designed with less shear reinforcement than the minimum requirement in the current design standards. The minimum shear reinforcement ratio, $\rho_{w,min}$, and the maximum spacing, s_{max}, have been introduced in the current design standards to prevent brittle failures, where, for example, the development of the critical shear crack immediately induces shear failure.[2–4] However, many existing concrete structures do not comply with these minimum requirements, and it is, therefore, not possible to account for the shear reinforcement when assessing the shear capacity. This leads to a lower estimated shear capacity than the design approach for members with a sufficient amount of shear reinforcement. Such structures require, in many cases, to be strengthened or even replaced to ensure adequate calculated load-bearing capacity.

It is well-known that the shear failure of reinforced concrete beams without and with small amounts of shear reinforcement is characterized by the development of a critical shear crack.[5–8] After the development of the critical shear crack, the shear capacity is governed by the contribution from several shear-transfer actions, such as aggregate interlock, the inclination of the compression chord, residual tensile stresses, shear reinforcement, and dowel action. The development of Digital Image Correlation (DIC) measurement systems has enabled detailed measurements of the shape and the kinematics of the critical shear crack. From these measurements on the surface of RC beams, estimates of the shear force carried by each of these potential shear-transfer actions can be performed.[5–14] In recent years, several more refined mechanical models have been proposed for estimating the shear capacity of RC beams that consider the contribution from each of the potential shear-transfer actions based on an assumed shape and kinematics of the critical shear crack.[10,15–19] This includes models that cover the transition from members without to members with small amounts of shear reinforcement.[20,21] In this context, the contribution from dowel action is often considered a constant shear contribution governed by the splitting strength of the concrete cover. Dowel tests previously reported in the literature for members without a tensile activation of the longitudinal reinforcement have shown that the shear contribution from dowel action remains constant after dowel cracking.[22–25] However, in a recent experimental campaign of dowel tests with a realistic activation of the longitudinal reinforcement, it was shown that the shear contribution from dowel action is significantly influenced by the level of tension in the reinforcement.[26] In that program, the response of members with a realistic activation of the longitudinal reinforcement ($\sigma_s \geq 130$ MPa) showed to be governed by a linear elastic regime, followed by a nonlinear regime with reduced stiffness. In fact, the longitudinal reinforcement, acting as a dowel, allows for additional stirrups that are not intercepted by the inclined part of the critical shear crack to be activated (see Figure 1). Dowelling action is, thus, potentially a key aspect to understand how the shear reinforcement is activated and its eventual contribution. As a consequence, dowelling action is a parameter to be considered together with the amount of shear reinforcement to prevent crack localization.

In this article, a novel mechanical model for calculating the shear force carried by dowel action is presented. The model covers both members with and without shear reinforcement and includes the contribution from the shear reinforcement. The mechanical model is an extension of the linear elastic dowel model presented and compared to dowel tests with a realistic activation of the tensile reinforcement.[26] The shear contribution from the

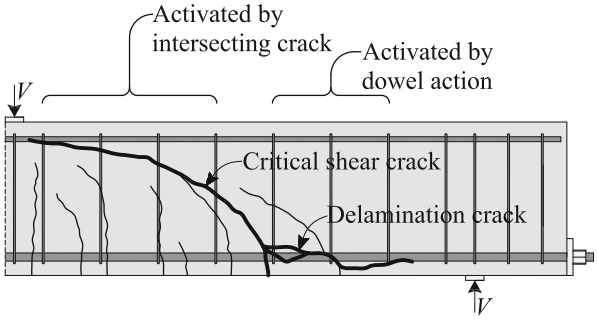

FIGURE 1 Stirrups activated by the intersecting critical shear crack and by dowel action of the tensile reinforcement.

mechanical dowel model depends on the crack kinematics and is developed to be implemented in advanced shear capacity models based on an assumed behavior for the crack kinematics of the critical shear crack, such as References 10,16–19. In addition, a detailed investigation of the influence of small amounts of shear reinforcement on the shear-transfer actions in RC beams is presented. The investigation is performed on the basis of DIC measurements of 16 shear tests of beams without and with small amounts of shear reinforcement from the experimental program by Autrup et al.[8,27] Constitutive models from the literature are adopted to estimate the remaining shear-transfer actions.

The investigation shows that the sum of the estimated shear force carried by the potential shear-transfer actions fairly well predicts the applied shear force from the development of the critical shear crack until failure. Additionally, for beams with shear reinforcement below the minimum requirements according to Eurocode 2,[2] it is shown that the contribution from aggregate interlock, residual tensile stresses, and the inclination of the compression chord governs the shear capacity. While for beams with shear reinforcement above the minimum requirements, the contribution from the shear reinforcement and dowel action governs the shear capacity.

Note that in Section 2, a brief extract/summary of the experimental program from Autrup et al.[8] is provided to facilitate readability.

2 | EXPERIMENTAL PROGRAM

In the following, the experimental program and the results are briefly presented. For a more thorough description, the reader is referred to Autrup et al.[8,27] The program consisted of 30 shear tests on 15 beams without and with small amounts of shear reinforcement. In the program, the diameter and the spacing of the stirrups (ϕ_w and s) and effective depth, d, were varied. Figure 2 shows details of the beams.

All beams were designed with a rectangular cross section with a shear span to an effective depth ratio $a/d = 3.4$ and a longitudinal reinforcement ratio $\rho_l =$ $1.25\% - 1.27\%$. The tensile reinforcement, ϕ_{lt}, consisted of three reinforcing bars, while the compressive reinforcement, ϕ_{lc}, consisted of two reinforcing bars, both scaled according to the beam size. Additionally, the ratio between the effective and total beam height $d/h = 0.88$. The minimum shear reinforcement ratio was $\rho_{w,min} \approx 0.1\%$, according to Eurocode 2[2] and *fib* Model Code 2010.[3] Table 1 shows the geometry of the beams, the reinforcement layout and the tested shear capacities.

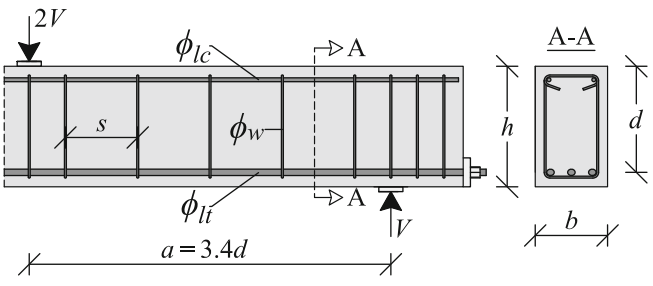

FIGURE 2 Test setup and details of the geometry and the reinforcement layout.

Two shear tests were performed for each beam, denoted A and B (corresponding to shear spans A and B). In shear test A, the shear reinforcement consisted of less ductile shear reinforcement compared to shear test B, corresponding to mainly ductility class A and C according to Eurocode 2.[2] Figure 3a, b shows the stress–strain curves for a representative tensile test of each size of shear reinforcement in shear tests A and B, respectively.

Table 2 shows the average tested mechanical properties of the shear reinforcement. Table 3 shows the average tested mechanical properties of the longitudinal tensile and compressive reinforcement. All beams were cast with normal-strength concrete made from the same recipe with a maximum aggregate size $d_g = 16$ mm. During the tests, full-field displacement measurements of the surface of the specimens were conducted by applying a three-dimensional DIC system. For a description of the DIC measuring system, the reader is referred to Reference 8.

3 | EVALUATION OF SHEAR-TRANSFER ACTIONS BASED ON DIC MEASUREMENTS

It is well-known that shear failure of reinforced concrete beams without and with low amounts of shear reinforcement is governed by the development of a critical shear crack.[5–8,10] By considering a free body defined by the critical shear crack (see Figure 4) and from measurements of the kinematics of the critical shear crack, the contribution from each of the potential shear-transfer actions can be estimated by applying suitable constitutive models. The shear-transfer actions can be summarized as:

1. The vertical component of aggregate interlock, V_{ag}
2. The vertical component of the residual tensile stresses, V_{res}
3. Tensile force in the vertical shear reinforcement, V_s
4. The vertical component of the inclined compression chord, V_{cc}
5. Dowel action of the tensile reinforcement, $V_{dow,t}$
6. Dowel action of the compressive reinforcement, $V_{dow,c}$

In the following, the method for estimating the crack kinematics from the DIC measurements and the

TABLE 1 Geometrical and material data of beams and tested shear capacities.

Specimen	d (mm)	ϕ_w (mm)	s (mm)	b (mm)	ϕ_{lt} (mm)	ϕ_{lc} (mm)	ρ_w (%)	f_c (MPa)	$V_{u,A}$ (kN)	$V_{u,B}$ (kN)
B.33.00.00	330	–	–	225	3Ø20	2Ø12	–	41.0	89.3	89.4
B.44.00.00	440	–	–	300	3Ø26.5	2Ø16	–	40.0	143.7	148.7
B.55.00.00	550	–	–	375	2Ø36 + 1Ø26.5	2Ø20	–	38.1	196.8	217.1
B.66.00.00	660	–	–	450	3Ø40	2Ø25	–	38.9	262.2	286.4
B.33.06.23	330	6	225	225	3Ø20	2Ø12	0.11	40.7	126.5	123.1
B.44.08.30.1	440	8	300	300	3Ø26.5	2Ø16	0.11	41.4	214.5	165.8
B.44.08.30.2	440	8	300	300	3Ø26.5	2Ø16	0.11	42.2	180.9	211.1
B.55.10.38	550	10	375	375	2Ø36 + 1Ø26.5	2Ø20	0.11	43.0	263.4	305.7
B.66.12.45	660	12	450	450	3Ø40	2Ø25	0.11	41.6	389.9	384.8
B.44.06.19	440	6	187.5	300	3Ø26.5	2Ø16	0.10	41.5	221.4	169.7
B.44.06.30.1	440	6	300	300	3Ø26.5	2Ø16	0.06	42.7	142.5	156.8
B.44.06.30.2	440	6	300	300	3Ø26.5	2Ø16	0.06	42.1	146.0	155.8
B.44.06.38	440	6	375	300	3Ø26.5	2Ø16	0.05	38.0	132.9	146.6
B.44.06.50	440	6	500	300	3Ø26.5	2Ø16	0.04	37.1	144.5	152.8
B.44.10.30	440	10	300	300	3Ø26.5	2Ø16	0.17	40.8	240.1	242.6

Note: The uniaxial concrete compressive strength f_c is based on the test of 100 × 200 mm cylinders and multiplied with a correction factor of 0.97 to obtain the equivalent strength of 150 × 300 mm cylinders (Nielsen[28]).

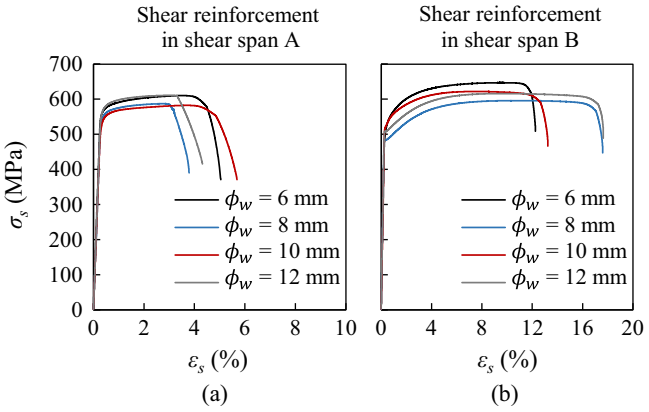

FIGURE 3 Tested stress–strain curves for a representative tensile test of each size of (a) shear reinforcement in span A and (b) shear reinforcement in span B.

constitutive models applied in this article are briefly presented. For the contribution of dowel action, a novel mechanical model is established in Section 4 for beams with and without shear reinforcement. The mechanical dowel model is an extension of the model presented in Autrup et al.[26] for beams without shear reinforcement.

3.1 | Measuring the crack kinematics

The crack kinematics are determined from the DIC measurements by adapting the methodology of Gehri et al.[29,30] similar to the approach by Campana et al.[5] Here, the shape of the crack is determined from the photogrammetric measurements and approximated by a polygonal line with a spacing of approximately two to three times the maximum aggregate size between each point. Subsequently, the polygonal line is subdivided into linear segments with a length of approximately 2 mm (see Figure 5a). For each line segment, the angle and the length are determined. At the midpoint of each line segment (referring to point O in Figure 5a), the crack kinematics are determined from four closely spaced reference points A_1, A_2, B_1 and B_2 located in the vicinity of the line segment. The four reference points are grouped into two pairs, pair A, located on side A of the crack and pair B, located on side B of the crack. By assuming a rigid-body displacement of sides A and B of the crack, the crack lip displacement of point O of each side of the crack (δ_A and δ_B) is determined from the displacement vectors (δ_{A1}, δ_{A2}, δ_{B1} and δ_{B2}) of the reference points. From the crack lip displacement of each side of the crack, the crack displacement vector δ is determined and decomposed into crack opening, w, and shear slip, δ_t, by including the influence of the crack lip rotation of each side of the crack (see Figure 5b).

3.2 | Aggregate interlock

In the literature, several constitutive models have been proposed to estimate the contact stresses developing

TABLE 2 Average tested mechanical properties of shear reinforcement.

	Shear reinforcement in shear span A				Shear reinforcement in shear span B			
ϕ_w (mm)	6	8	10	12	6	8	10	12
f_y (MPa)	577	558	554	582	525	481	530	508
E_s (GPa)	203	198	195	195	199	206	202	203
f_u (MPa)	615	585	585	612	641	593	620	615
ε_{s0} (%)	3.9	2.9	3.7	3.3	8.7	10.5	7.1	9.0
ε_{su} (%)	5.2	4.1	5.4	5.3	11.0	15.8	10.2	13.0

Note: ε_{s0} denotes the strain at the maximum stress and ε_{su} denotes the maximum strain before rupture.

TABLE 3 Average tested mechanical properties of longitudinal reinforcement.

	Tensile reinforcement				Compressive reinforcement			
$\phi_{lt/lc}$ (mm)	20	26.5	36	40	12	16	20	25
f_y (MPa)	983	995	987	950*	571	590	574	586
E_s (GPa)	186	210	214	210*	197	192	200	197
f_u (MPa)	1170	1102	1102	1050*	655	688	659	682
ε_{s0} (%)	4.2	7.9	8.6	–*	8.3	8.7	9.5	9.3
ε_{su} (%)	7.8	10.4	11.6	–*	10.8	12.3	15.0	14.7

Note: ε_{s0} denotes the strain at the maximum stress and ε_{su} denotes the maximum strain before rupture.
*Nominal values, but expected to be similar to the tested values for ϕ_l 26.5 and 36 mm.

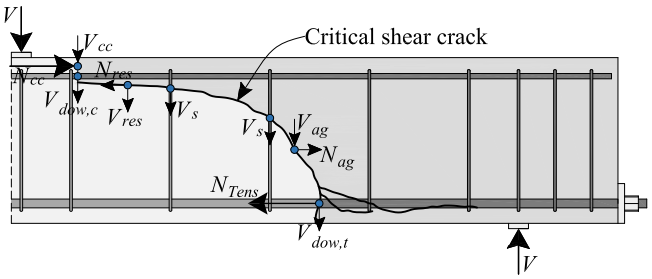

FIGURE 4 Forces acting on the free body defined by the critical shear crack.

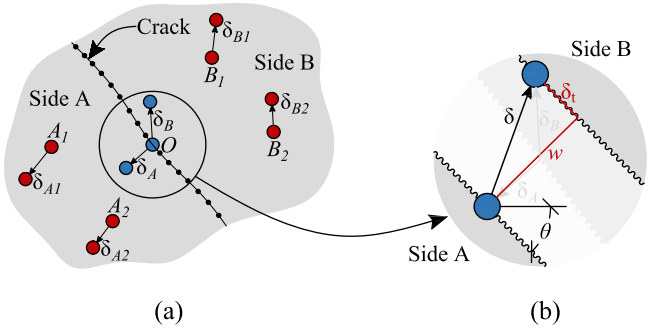

FIGURE 5 (a) Details of the measurement points used to determine the crack kinematics and (b) decomposition of crack lip displacement into the crack opening, w, and shear slip, δ_t.

between crack surfaces due to aggregate interlock, dependent on the crack opening w, the shear slip δ_t, and the crack surface roughness.[10,31–37] However, at large crack openings, these models tend to overestimate the aggregate interlock stresses. Therefore, in this article, the modified aggregate interlock model proposed by Autrup et al.[8] is applied. This expression has been shown to accurately predict the aggregate interlock stresses for Mixed-Mode tests,[34,38–40] even at large crack openings, which are especially relevant for beams with shear reinforcement. The approach to determine the shear force carried by aggregate interlock from the measured crack kinematics is described in Autrup et al.[8]

3.3 | Residual tensile stresses

The shear force carried by the residual tensile stresses in the fracture process zone (FPZ)[41] is determined according to the expression by D. A. Hordijk,[42] by the approach described by Autrup et al.[8]

3.4 | Shear reinforcement

In the literature, several models have been proposed to estimate the bond-slip relation.[43–46] In this article, the activation of the shear reinforcement is determined from

the measured crack opening in the direction of the shear reinforcement by adapting the simple rigid-perfectly plastic bond-slip relation according to the Tension Chord Model (TCM) by Marti et al.[47] Additionally, for the shear reinforcement, a bilinear stress–strain relation is adopted. This approach is further described in Autrup et al.[8] and has been shown by the authors and others to accurately predict the imposed tensile stress from a measured crack opening.

The propagation of the critical shear crack in a reinforced concrete beam involves horizontal delamination cracks along the compressive and tensile reinforcement (see Figure 4). Along these cracks, the contribution from the shear reinforcement is not directly related to the measured crack opening. Rather, at these locations, the shear reinforcement contributes indirectly by affecting the shear-transferring mechanism of dowel action of the tensile and compressive reinforcement (see Section 4). Therefore, in the following, only stirrups that are intersected by the inclined branch of the critical shear crack between the compressive and tensile reinforcement is included using the approach outlined in Autrup et al.[8]

3.5 | The inclination of the compression chord

In the uncracked compression zone, shear can be transferred by the inclination of the compression chord. The size and the inclination of the compression chord can be estimated from the measured principal strains determined from the photogrammetric measurements performed specifically on a small area in the compression zone.[10] Due to the lack of such measurements and a relatively small contribution for slender beams ($a/d > 2.5$) at maximum load,[5,15] the simplified analytical approach proposed by Cavagnis et al.[48] is applied. Note that this approach is only for load stages where the critical shear crack has developed close to the compression zone. Figure 6a shows details of the assumed stress distribution in the compression zone. At the tip of the critical shear crack and towards the top of the beam, a linear elastic stress distribution is assumed. The horizontal compressive resultant is thus located at $c_n = h_F/3$ measured from the top of the beam, where h_F is the height of the uncracked compression zone. Compressive stresses equal to f_c are assumed below the loading plate. The inclination of the compressive chord can, therefore, be expressed as:

$$\alpha_{cc} = \arctan\left(\frac{c_n - c_m}{r_{F,edge}}\right) \geq \frac{1}{3}\alpha_{cr} \tag{1}$$

where c_n (h_F) and $r_{F,edge}$ are determined from the photogrammetric measurements. Additionally, the inclination of the compression chord is limited to 13 of the angle α_{cr} to account for the geometrical limitation of the shape of the critical shear crack (see Figure 6b), where the angle α_{cr} is determined by the tangent to the critical shear crack from the tip of the crack. The latter limit becomes governing for members where the critical shear crack develops either horizontally or close to the loading plate.

The horizontal component of the compression chord, N_{cc}, is, thus, determined from a horizontal and rotational equilibrium, including the applied shear force and all the acting shear-transfer actions (see Figure 4). The height of the compression zone, c_m, is obtained as:

$$c_m = \frac{N_{cc}}{2 \cdot b \cdot f_c} \tag{2}$$

The vertical component of the inclined compression chord is then determined as:

$$V_{cc} = N_{cc} \cdot \tan(\alpha_{cc}) \tag{3}$$

4 | NOVEL MODELING APPROACH FOR DOWEL ACTION

In the following, a linear-elastic mechanical model for dowel action of the tensile and compressive reinforcement is proposed. The model covers beams with and without shear reinforcement and includes the contribution from the shear reinforcement activated by dowel

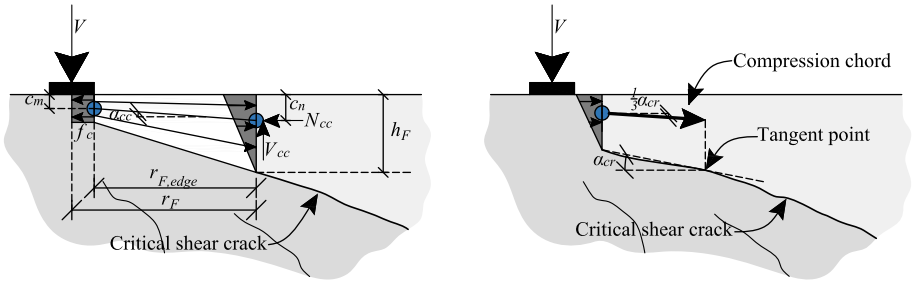

FIGURE 6 (a) Assumed stress distribution in the compression zone according to Cavagnis et al.,[48] and (b) geometrical limitation of the inclination of the compression chord.

action. The model is established by assuming a displacement function for the dowel and by applying the work equation on the rates of internal and external works. Additionally, a method for extracting the dowel displacement from the DIC measurements is presented based on the approach by Autrup et al.[26] Finally, a rigid-plastic dowel model is presented to serve as an upper limit for the shear force carried by dowel action.

4.1 | Measuring the dowel displacement

In the following, the method to determine the dowel displacement from the DIC measurements is presented. The method is developed by assuming a rigid-body displacement for the concrete on both sides of the shear and dowel crack. The dowel displacement is determined from four measuring points A_1, A_2, B_1, and B_2 located in the DIC displacement field (see Figure 7a, b).

The measuring points are grouped into displacement points (A_1 and B_1) and rotation points (A_2 and B_2), where the indices A and B refer to points located on side A and B of the shear and dowel crack, respectively. In the undeformed state, the coordinates of the measuring points are referred to as A_1, A_2, B_1, and B_2, whereas in the deformed state, the coordinates of the measuring points are referred to as δ_{A1}, δ_{A2}, δ_{B1}, and δ_{B2}. The rigid body rotation of sides A and B of the shear and dowel crack is expressed as:

$$\theta_A = \arctan\left(\frac{\delta_{A1,y}-\delta_{A2,y}}{\delta_{A1,x}-\delta_{A2,x}}\right) - \arctan\left(\frac{A_{1,y}-A_{2,y}}{A_{1,x}-A_{2,x}}\right) \quad (4)$$

$$\theta_B = \arctan\left(\frac{\delta_{B2,y}-\delta_{B1,y}}{\delta_{B2,x}-\delta_{B1,x}}\right) - \arctan\left(\frac{B_{2,y}-B_{1,y}}{B_{2,x}-B_{1,x}}\right) \quad (5)$$

where the subscripts x and y denote the x- and y-coordinates of the associated measuring point. The vertical displacements of sides A and B of the dowel (Δ_{Ay} and $\Delta_{By,i}$ in Figure 7) are determined as:

$$\Delta_{Ay} = A_y - \delta_{A1,y} - \cos(\theta_A)\left(A_y - A_{1,y}\right) - \sin(\theta_A)(A_x - A_{1,x}) \quad (6)$$

$$\Delta_{By,i} = B_y - \delta_{B1,y} - \cos(\theta_B)\left(B_y - B_{1,y}\right) - \sin(\theta_B)(B_{x,i} - B_{1,x}) \quad (7)$$

where A_x and A_y describe the x- and y-coordinates of dowel point A (left endpoint) and $B_{x,i}$ and B_y describe the x- and y-coordinates of dowel point B (right endpoint) in the undeformed state. Note that points A and B are placed such that the y-coordinate correspond to the midpoint of the dowel in the undeformed state. Figure 7a, b shows the definition of the x-coordinates. Here, A_x is determined from the x-coordinate of the intersection between the shear crack and the midpoint of reinforcement ($A_x = A_{x,cr} - l_{cc}$). For beams with shear reinforcement, parameter $B_{x,i}$ is determined from the x-coordinate of the intersection between the shear crack and the reinforcement and the distance to the first stirrup ($B_{x,i} = A_{x,cr} + x_w + (i-1)s$), where the subscript i refers to the deformation phase of the dowel displacement (number of stirrups activated by dowel action due to the dowel displacement). For beams without shear reinforcement, the parameters A_x and $B_{x,i}$ are determined from the x-coordinate of the intersection between the dowel and shear crack or dowel crack, respectively, expressed as $A_x = A_{x,cr} - l_{cc}$ and $B_{x,i} = B_{x,cr} + l_{cc}$ (see Figure 7b). The length l_{cc} is determined from consideration of rotational

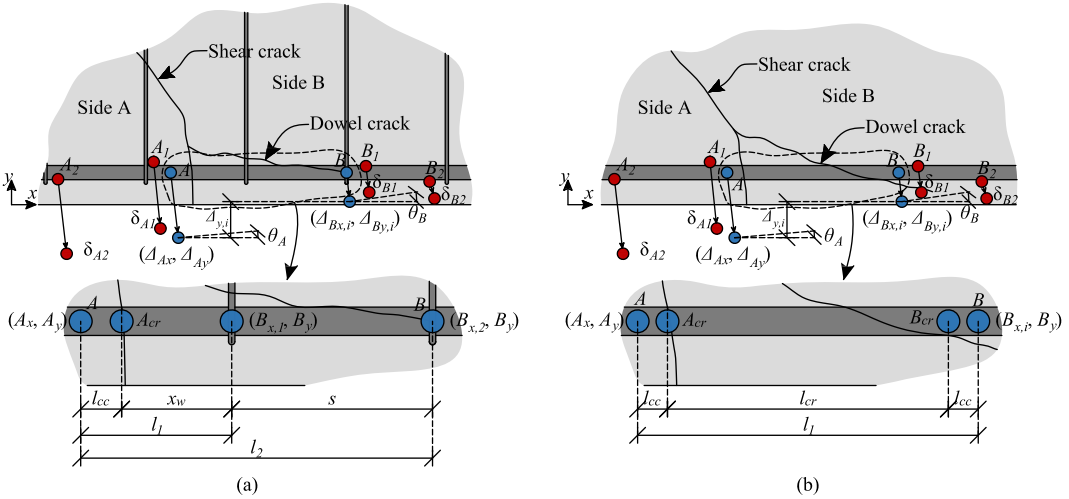

FIGURE 7 Details of the measurement points for determining the dowel displacement, Δ_y, for (a) a beam with shear reinforcement and (b) a beam without shear reinforcement.

and vertical equilibrium in the plastic state (further described in Section 4.3). The position of both $A_{x,cr}$ and $B_{x,cr}$ can be determined from the DIC measurements. The length of the free dowel is obtained as:

$$l_i = B_{x,i} - A_x \tag{8}$$

The vertical displacement of the dowel, $\Delta_{y,i}$, in phase i is, thus, determined as:

$$\Delta_{y,i} = \Delta_{Ay} - \Delta_{By,i} \tag{9}$$

Note that the horizontal displacement, $\Delta_{x,i}$, of the dowel is not considered, as this displacement is assumed to relate to the bending moment in the reinforced concrete beam.

4.2 | Elastic dowel model

For beams with and without shear reinforcement, the model for the shear contribution from dowel action is generally the same. During the propagation of the dowel crack in beams with shear reinforcement and until the dowel crack intersects the first stirrup, the contribution from dowel action is determined according to the approach for members without shear reinforcement. For a beam without shear reinforcement, the displacement of the dowel is assumed to be described by one third-order polynomial (see Figure 8a), where the length of the dowel is mainly governed by the horizontal dowel crack length determined by the photogrammetric measurements (see Figure 8b). For beams with shear reinforcement, the displacement of the dowel is assumed to be described by the sum of i third-order polynomials, where i refers to the deformation phase of the dowel displacement (see Figure 8c). The ith third-order polynomial is assumed to develop between point A (referring to Figure 8c) and the ith stirrup from point A. In deformation phase, i the total dowel displacement, $\Delta_{y,i}$, is determined as:

$$\Delta_{y,i} = \sum_{j=1}^{i} \delta_{y,j} \tag{10}$$

where $\delta_{y,j}$ is the local dowel displacement of the jth third-order polynomial (see Figure 8a–c).

The displacement of the stirrups (elongation) is assumed equal to the displacement of the dowel at the location of the stirrups. This assumption is of course only valid for members where the dowel is located close to the vertical legs of the shear reinforcement. Additionally, for the shear reinforcement, a rigid-perfectly plastic load–displacement relation is assumed. By applying the TCM by Marti et al.,[47] it can be shown that the dowel displacement that induces yielding in ordinary stirrups (i.e., ribbed reinforcement with $\phi_w = 6 - 10\,\text{mm}$ and $f_{yw} = 550\,\text{MPa}$) embedded in normal strength concrete is very small, i.e. $w_{cr,y} < 0.3\,\text{mm}$ (for other scenarios, such as smooth shear reinforcement, this assumption may not always be correct).

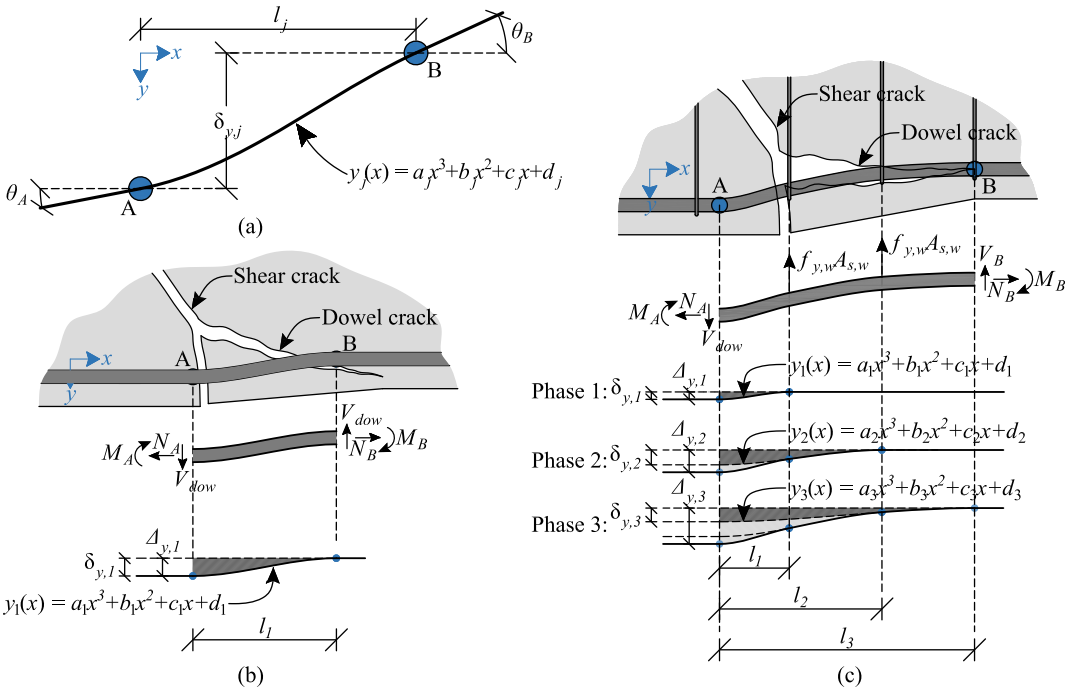

FIGURE 8 (a) Details of the geometrical properties of the dowel displacement, $\delta_{y,j}$, and dowel rotation θ_B and θ_A, (b) dowel action for a beam without shear reinforcement, and (c) dowel action for a beam with shear reinforcement.

The dowel response is modeled by incrementally applying the work equation, for an infinitesimal incremental dowel displacement, $\dot{\Delta}_{y,i}$. Here, a balance is established between the incremental work performed by the dowel force, $\dot{W}_E$, (see Figure 9a) and the incremental internal work, $\dot{W}_I$. The incremental internal work consists of a contribution from the stored elastic energy in the dowel, $\dot{W}_{I,d}$ (see Figure 9b) and a contribution from the dissipated energy from the shear reinforcement, $\dot{W}_{I,w}$ (see Figure 9c). Note that the contribution from residual tensile stresses is not included, which at low-stress levels of the tensile reinforcement increases the shear force carried by dowel action.[26] For the distribution of the total dowel displacement, $\Delta_{y,i}$, into the local dowel displacements, $\delta_{y,j}$, a minimum of internal work is only obtained if in deformation phase i only the local dowel displacement, of the ith third-order polynomial increases (see Figure 8c), that is, $\dot{\delta}_{y,i} = \dot{\Delta}_{y,i}$. This minimum of internal work and the distribution of the dowel displacement is based on the assumption of a rigid-perfectly plastic load–displacement relation for the shear reinforcement.

4.2.1 | External incremental work

For an infinitesimal incremental dowel displacement, $\dot{\Delta}_{y,i}$, the incremental external work (see Figure 8b, c and Figure 9a) can be expressed as:

$$\dot{W}_E = V_{dow} \cdot \dot{\Delta}_{y,i} \tag{11}$$

Note that the sectional axial forces, N_A and N_B, the bending moments, M_A and M_B, and the shear force, V_B, (see Figure 8b, c) are not included because the associated displacement rates are assumed zero (assumed not to relate to the shear force carried by dowel action).

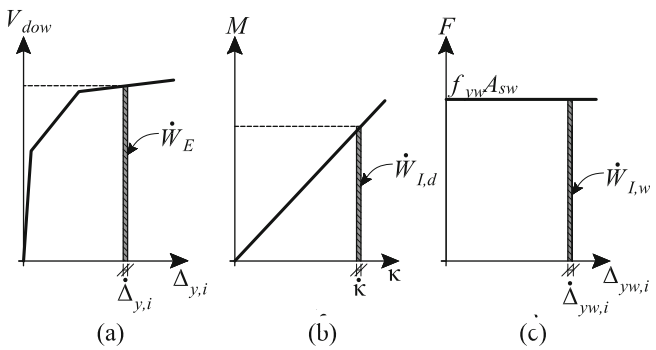

FIGURE 9 (a) Incremental external work, (b) incremental internal work in the dowel, and (c) incremental internal work in the stirrups.

4.2.2 | Incremental internal work in dowel

In the elastic deformation phase i, the displacement of the dowel is assumed to be described by the sum of i third-order polynomials. The displacement described by the j'th third-order polynomial (see Figure 8a) can be expressed as:

$$y_j(x) = a_j x^3 + b_j x^2 + c_j x + d_j \tag{12}$$

The geometrical boundary conditions for the dowel displacement are decomposed into a contribution from the transverse dowel displacement, $\delta_{y,j}$, and a contribution from the rotation of the dowel, θ_A and θ_B (see Figure 10). The boundary conditions for the contribution from the transverse dowel displacement is $y_j(0) = \delta_{y,j}$ and $y_j(l_j) = y_j'(0) = y_j'(l_j) = 0$. By assuming small displacements $\tan(\theta_A) \approx \theta_A$; hence, the boundary conditions for the contribution from the rotation of the dowel are $y_j(0) = y_j(l_j) = 0$, $y_j'(0) = -\theta_A$, and $y_j'(l_j) = -\theta_B$. Solving Equation (12) with the four boundary conditions for both the contribution from the transverse dowel displacement and the rotation, the displacement functions of the jth third-order polynomial are obtained as:

$$y_{j,t}(x) = 2\frac{\delta_{y,j}}{l_j^3}x^3 - 3\frac{\delta_{y,j}}{l_j^2}x^2 + \delta_{y,j} \tag{13}$$

$$y_{j,r}(x) = -\frac{\theta_A + \theta_B}{l_j^2}x^3 + \frac{2\theta_A + \theta_B}{l_j}x^2 - \theta_A x \tag{14}$$

where the subscripts t and r denote the transverse dowel displacement and the rotation, respectively. As small displacements are assumed $dx/ds \approx 1$ and $\kappa \approx d\theta(x)/dx$. Additionally, by assuming that the length of the dowel is much longer than the diameter, the contribution from the shear deformation in the dowel is negligible. The

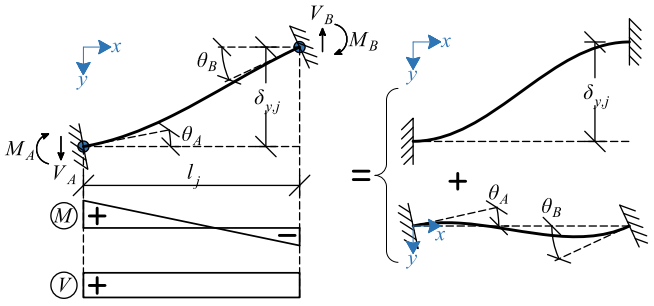

FIGURE 10 Decomposition of the dowel displacement into a contribution from the transverse dowel displacement, $\delta_{y,j}$, and a contribution from the rotation, θ_A and θ_B, at points A and B, respectively.

incremental internal work in the dowel (stored due to elastic deformation) in the deformation phase i can be expressed as:

$$\dot{W}_{I,d} = \sum_{j=1}^{i} \int_0^{l_j} M_j(x)\dot{\kappa}_j(x)dx \tag{15}$$

where i is the deformation phase, j is the index number for each of the third-order polynomials, $M_j(x) = M_{j,t}(x) + M_{j,r}(x)$ and is the bending moment imposed by the jth third-order polynomial and is composed of contributions from the transverse dowel displacement ($M_{j,t}(x)$) and the rotation ($M_{j,r}(x)$) and $\dot{\kappa}_j(x)$ is the incremental curvature of the j'th third-order polynomial. Note that the contribution from the rotation of the dowel is only determined from the ith third-order polynomial (the deformation phase), as a minimum of internal stored elastic energy is only obtained if the rotational boundary conditions develop for the longest dowel length (l_i). From the Bernoulli beam theory, the bending moment along the dowel can be determined as:

$$M(x) = E_{sl} \cdot I_l \frac{d^2 y(x)}{dx^2} \tag{16}$$

where $I_l = \pi\phi_l^4/64$ is the area moment of inertia and ϕ_l is the diameter of the dowel. From the displacement functions and the Bernoulli beam theory, the bending moment along the dowel can be expressed as:

$$M_{j,t}(x) = E_{sl} \cdot I_l \left(12\frac{\delta_{y,j}}{l_j^3}x - 6\frac{\delta_{y,j}}{l_j^2} \right) \tag{17}$$

$$M_{i,r}(x) = E_{sl} \cdot I_l \left(-6\frac{\theta_A + \theta_B}{l_i^2} + 2\frac{2\theta_A + \theta_B}{l_i} \right) \tag{18}$$

As already mentioned, a minimum of internal work is obtained if in the deformation phase i only the local dowel displacement, $\delta_{y,i}$, of the i'th third-order polynomial increases, i.e. a minimum of internal incremental work is obtained if the incremental displacement $\dot{\Delta}_{y,i}$ only increases the local dowel displacement, $\delta_{y,i}$, that is, $\dot{\Delta}_{y,i} = \dot{\delta}_{y,i}$. Therefore, in the deformation phase i, the incremental curvature can be expressed as:

$$\dot{\kappa}_j(x) = \frac{d^2 \dot{y}_{i,t}(x)}{dx^2} = 12\frac{\dot{\Delta}_{y,i}}{l_i^3}x - 6\frac{\dot{\Delta}_{y,i}}{l_i^2} \tag{19}$$

By inserting Equation (17), Equation (18), and Equation (19) into Equation (15), the following solution is obtained:

$$\dot{W}_{I,d} = \sum_{j=1}^{i} E_{sl} \cdot I_l \cdot n_l \left(12\frac{\delta_{y,j}}{l_i^3}\dot{\Delta}_{y,i} - 6\frac{\theta_A + \theta_B}{l_i^2}\dot{\Delta}_{y,i} \right) \tag{20}$$

where n_l is the number of dowels. From Equation (10), Equation (20) can be expressed as:

$$\dot{W}_{I,d} = E_{sl} \cdot I_l \cdot n_l \left(12\frac{\Delta_{y,i}}{l_i^3}\dot{\Delta}_{y,i} - 6\frac{\theta_A + \theta_B}{l_i^2}\dot{\Delta}_{y,i} \right) \tag{21}$$

4.2.3 | Internal incremental work in stirrups

From the assumption of a rigid-perfectly plastic load–displacement relation for the stirrups, the incremental internal work dissipated by the stirrups is determined as:

$$\dot{W}_{I,w} = \sum_{j=1}^{i} f_{y,w} A_{s,w} \dot{\Delta}_{yw,ji} \tag{22}$$

where $\dot{\Delta}_{yw,ji}$ is the incremental elongation of the stirrup j in the deformation phase i. As previously mentioned, a minimum of internal work is obtained if in the deformation phase i only the displacement of the ith third-order polynomial increases. The incremental displacement of the stirrup j in phase i can, therefore, be determined from Equation (13) as:

$$\dot{\Delta}_{yw,ji} = 2\frac{\dot{\Delta}_{y,i}}{l_i^3}l_j^3 - 3\frac{\dot{\Delta}_{y,i}}{l_i^2}l_j^2 + \dot{\Delta}_{y,i} = \frac{(l_i - l_j)^2(l_i + 2l_j)}{l_i^3}\dot{\Delta}_{y,i} \tag{23}$$

In the deformation phase i, the incremental internal work in the stirrups can, therefore, be expressed as:

$$\dot{W}_{I,w} = \sum_{j=1}^{i} f_{y,w} A_{s,w} \frac{(l_i - l_j)^2(l_i + 2l_j)}{l_i^3}\dot{\Delta}_{y,i} \tag{24}$$

4.2.4 | Work equation

By setting up the work equation, that is, $\dot{W}_E = \dot{W}_{I,d} + \dot{W}_{I,w}$ the following solution is obtained:

$$V_{dow} = E_{sl} \cdot I_l \cdot n_l \left(12\frac{\Delta_{y,i}}{l_i^3} - 6\frac{\theta_A + \theta_B}{l_i^2} \right) + \sum_{j=1}^{i} f_{y,w} A_{s,w} \frac{(l_i - l_j)^2(l_i + 2l_j)}{l_i^3} \tag{25}$$

where n_l is the number of dowels. For members with different dowel sizes, the term $n_l E_{sl} I_l$ is substituted with the term $\sum_{j=1}^{n_l} E_{sl,j} I_{l,j}$, where $E_{sl,j}$ and $I_{l,j}$ are the Young's modulus and the second moment of area for the jth dowel, respectively. The deformation phase is then determined as the minimum solution to Equation (25). This is obtained by incrementally increasing the deformation phase i from zero and until $i+1$ results in a higher estimate. Similar results could also be obtained by adapting the load–displacement relation for the stirrups according to the TCM by Marti et al.[47] (but the increase in the complexity is not justified in terms of accuracy). In Appendix A, a simplified approach is presented for closely spaced stirrups, where the rigid-perfectly plastic load–displacement relation of the stirrups is assumed to act as an equivalent evenly distributed tensile stress along the dowel. Note that this expression is more suitable as a design expression, where the distance from the critical shear crack to the first stirrups is unknown, which has a significant influence on the shear contribution from dowel action.[23,24] Figure 11 shows the influence of the distance from the critical shear crack to the first stirrups, l_1, on the estimated shear force carried by dowel action according to Equation (25) and the simplified dowel model, $V_{dow,s}$, in Appendix A. Note that the rotation of the dowel θ_A and θ_B is zero, the shear reinforcement ratio $\rho_w = 0.112\%$, $f_{yw} = 500$ MPa, $\phi_l = 26.5$ mm, $n_l = 3$ and $E_{sl} = 200$ GPa, similar to the tests presented in Section 2. From the figure, it is observed that the stiffness of the response according to Equation (25) increases as the distance from the shear crack to the first stirrup decreases, whereas the simplified dowel model in Appendix A is not influenced by this distance.

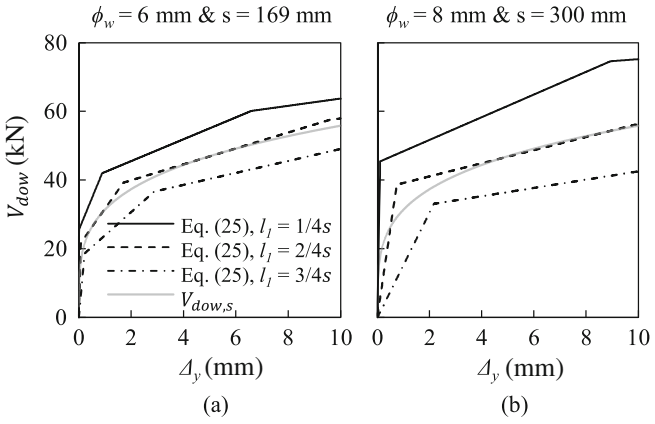

FIGURE 11 Influence of the distance from the critical shear crack to the first stirrups, l_1, on the estimated shear force carried by dowel action according to Equation (25) and the simplified dowel model, $V_{dow,s}$, in Appendix A.

4.3 | Plastic solution

For a sufficiently large dowel displacement, the bending moment in the dowel in the two sections with the largest bending moment will reach the plastic bending capacity and cause the development of two plastic hinges. In this plastic state, the dowel is assumed to behave rigid-perfectly plastic, where all the deformation localizes in the plastic hinges. The position of these plastic hinges coincides with points A and B in the elastic state (see Figure 8b, c) as the bending moment in the dowel reaches a maximum at these two sections in the elastic state. The position of points A and B can, therefore, be determined from the plastic solution at the initiation of pure dowel action by a rotational and horizontal equilibrium, similar to other approaches.[26,49–51] However, it should be noted that for small angles of the shear crack at the intersection with the dowel, the position of the endpoints potentially could be influenced by a breakout failure of the concrete (see, for example, Cantone et al.[52]). Figure 12a shows the forces acting on the dowel in the plastic state at the initiation of pure dowel action for a beam with shear reinforcement.

Point A is assumed to be located at a distance, l_{cc}, from the intersection with the shear crack and the dowel. Along the length, l_{cc}, a uniform contact pressure equal to f_c is assumed to develop, and in the stirrups, a tensile force equal to $f_{y,w}A_{s,w}$ is also assumed. From a rotational and vertical equilibrium for pure dowel action (see Figure 12a) the number of stirrups activated by dowel action, n_w, and the length of the uniform contact pressure, l_{cc}, are obtained when the force in the stirrup at point B, F_w, becomes less than the plastic tensile capacity of the stirrup, $A_{s,w}f_{y,w}$. The tensile force, F_w, and the length, l_{cc}, are expressed:

$$F_w = \left(\sqrt{(x_w + n_w s)^2 + \frac{(n_w^2 + n_w) A_{sw} f_{y,w} s + 4 M_p n_l}{f_c n_l \phi_l}} - x_w - n_w s_w \right) f_c n_l \phi_l - n_w A_{s,w} f_{y,w} \tag{26}$$

$$l_{cc} = \frac{F_w}{f_c n_l \phi_l} - n_w A_{s,w} f_{y,w} \tag{27}$$

The number of stirrups activated, n_w, is determined by incrementally increasing n_w from zero until F_w becomes less than $A_{s,w}f_{y,w}$, that is, the tensile stress in the last stirrups becomes less than the yield stress. The plastic bending capacity of the reinforcement, M_p, is determined as:

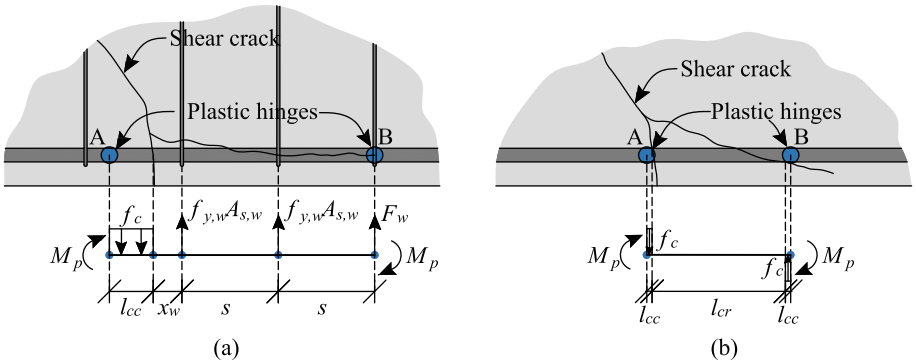

FIGURE 12 Details of the geometry and forces acting on the dowel at the initiation of pure dowel action for (a) a beam with shear reinforcement and (b) without shear reinforcement.

$$M_p = \frac{1}{6}\phi_l^3 f_y \tag{28}$$

Note that F_w and l_{cc} (Equation (26) and (27)) is determined from the full plastic bending capacity of the dowel. In reality, for tensile reinforcement, the bending moment in a beam induces a tensile force, thus reducing the plastic bending capacity of the dowel and inducing bond stresses in the concrete, which reduces the concrete compressive strength along the dowel. The interaction between the reduced plastic bending capacity of the dowel and the reduced concrete compressive strength is quite complex and is neglected for F_w and l_{cc}.

For beams without shear reinforcement the dowel length, l_1, is determined from the measured horizontal dowel crack length, l_{cr}, defined as the distance from the shear crack to the intersection between the reinforcement and the dowel crack (see Figure 12b). The horizontal length of the dowel crack is zero until dowel cracking occurs. However, during the propagation of the dowel crack, the length l_{cr} increases until the dowel crack is stable and the full length is reached. The dowel length, l_1, is determined from a rotational equilibrium at the initiation of pure dowel action in the plastic state. Points A and B of the plastic hinges are assumed to be located at a distance, l_{cc}, from the dowel crack length (see Figure 12b). Similarly to beams with shear reinforcement, along the length, l_{cc}, a contact pressure equal to f_c is assumed to develop. From a vertical and rotational equilibrium for pure dowel action, the length l_{cc} is determined as:

$$l_{cc} = \sqrt{\frac{l_{cr}^2}{4} + \frac{2M_p}{f_c \phi_l}} - \frac{l_{cr}}{2} \tag{29}$$

where the total dowel length is determined as $l_1 = l_{cr} + 2l_{cc}$. Note that the length, l_{cc} is determined from the full plastic bending capacity of the dowel, M_p. Furthermore, note that the length, l_{cc}, is only significant for the shear force carried by dowel action at the initiation of dowel cracking. The initiation of dowel cracking is, however, very brief and subsequently, the length, l_{cc}, becomes insignificant.

For beams with and without shear reinforcement, an upper limit for the maximum shear force carried by dowel action is introduced and determined as the plastic solution at the initiation of pure dowel action. The plastic solution is derived by considering the external and internal work due to an incremental dowel displacement at point A, shown in Figure 12, obtained as:

$$V_{dow,P} = \frac{2n_l M_p}{l_i} + \sum_{j=1}^{n_w} \frac{j \cdot s}{l_i} f_{y,w} A_{s,w} \tag{30}$$

where $i = 1$ for beams without shear reinforcement and $i = n_w$ for beams with shear reinforcement. However, it should be noted that in the plastic state, the dowel will undergo rotation and elongation for an increasing dowel displacement, which affects the plastic solution[26,51] which is not accounted for in the simple Equation (30). Additionally, for the tensile reinforcement in an RC beam, new plastic hinges may form for increasing loads than those determined from the simple Equation (30), as the imposed tensile force increases, thus reducing the plastic bending capacity of the reinforcement. Such a solution is, however, only relevant for members with a large shear reinforcement ratio, which requires large plastic deformations before reaching the ultimate load. Such a solution is, therefore, outside the scope of this paper.

5 | ANALYSIS OF EXPERIMENTS

In the following, the contributions from each of the five potential shear-transfer actions presented in Sections 3 and 4 are calculated on the basis of the DIC measurements for 16 selected beams of the total 30 tested beams presented by Autrup et al.[8,27] One specimen for each varying parameter in the experimental campaign. For specimens with shear reinforcement, only specimens with type B shear reinforcement are analyzed for each

varying parameter. Additionally, two specimens with type A shear reinforcement and $\rho_w > \rho_{w,min}$ are analyzed. In total, this includes specimens with a shear reinforcement ratio ranging from $\rho_w = 0.04\%$–0.17% and beams with an effective beam depth ranging from $d = 330$–660 mm for both beams with and without shear reinforcement.

5.1 | Calculated contributions from shear-transfer actions

Figures 13–20 show the measured crack kinematics at selected load stages, the measured load–displacement curves, and the calculated shear force carried by each of the potential shear-transfer actions for eight selected specimens. Note that the colored lines denote the measured relative displacement between the crack surfaces (crack kinematics), where the different line colors correspond to the load stage on the load–displacement curve with the marker of the same color. The size of the measured crack kinematics can be determined from the associated scale. In general, it can be observed that from the

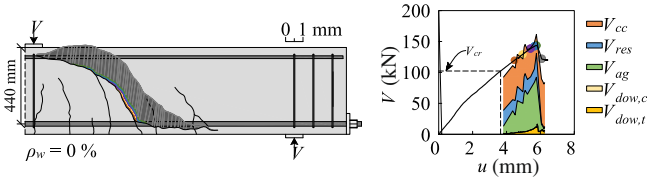

FIGURE 13 Measured crack kinematics at selected load stages and comparison of the measured load–displacement curve and calculated shear force carried by each shear-transfer action for beam B.44.00.00.A.

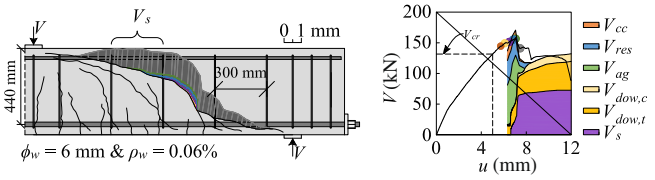

FIGURE 14 Measured crack kinematics at selected load stages and comparison of the measured load–displacement curve and calculated shear force carried by each shear-transfer action for beam B.44.06.30.1.B.

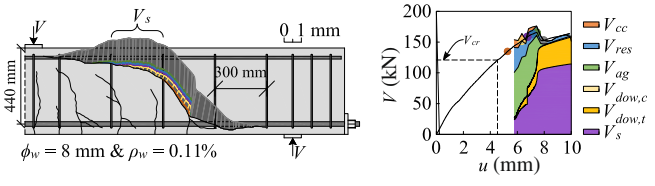

FIGURE 15 Measured crack kinematics at selected load stages and comparison of the measured load–displacement curve and calculated shear force carried by each shear-transfer action for beam B.44.08.30.1.B.

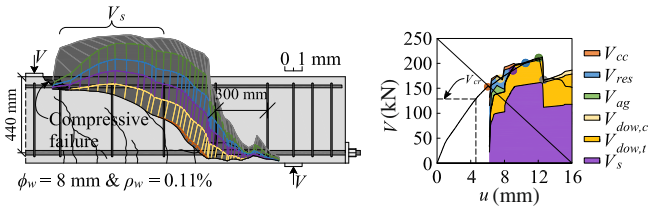

FIGURE 16 Measured crack kinematics at selected load stages and comparison of the measured load–displacement curve and calculated shear force carried by each shear-transfer action for beam B.44.08.30.2.B.

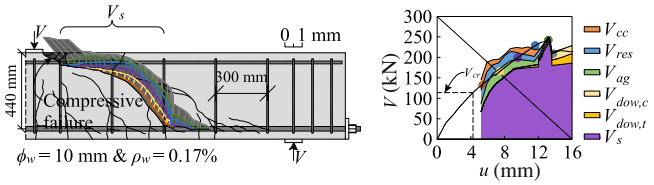

FIGURE 17 Measured crack kinematics at selected load stages and comparison of the measured load–displacement curve and calculated shear force carried by each shear-transfer action for beam B.44.10.30.B.

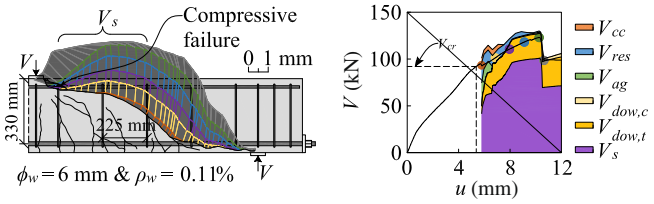

FIGURE 18 Measured crack kinematics at selected load stages and comparison of the measured load–displacement curve and calculated shear force carried by each shear-transfer action for beam B.33.06.23.B.

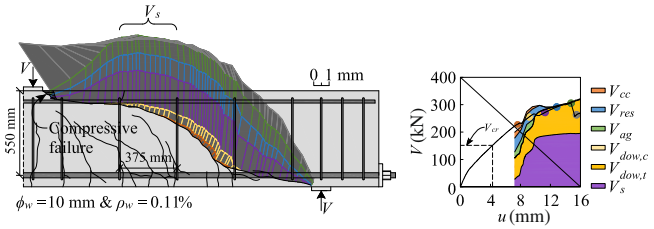

FIGURE 19 Measured crack kinematics at selected load stages and comparison of the measured load–displacement curve and calculated shear force carried by each shear-transfer action for beam B.55.10.38.B.

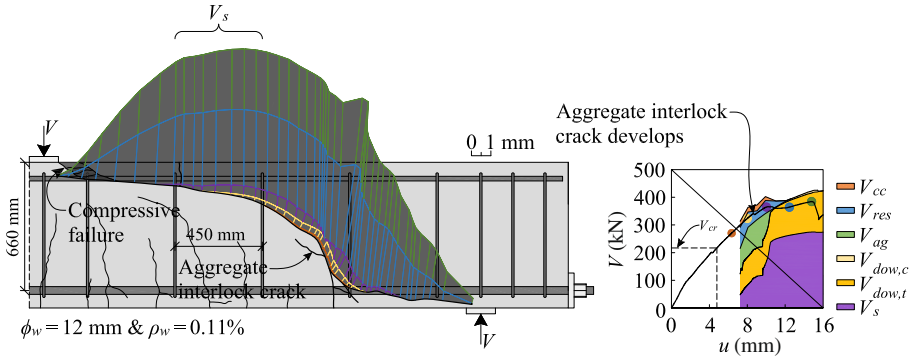

FIGURE 20 Measured crack kinematics at selected load stages and comparison of the measured load–displacement curve and calculated shear force carried by each shear-transfer action for beam B.66.12.45.B.

development of the critical shear crack and until failure, the calculated sum of shear force carried by each of the potential shear-transfer actions fairly well predicts the applied shear force.

For specimen B.44.00.00.A without shear reinforcement (Figure 13), the calculated shear force carried by the residual tensile stresses and the inclination of the compression chord were almost constant from the development of the critical shear crack until failure. While the contribution from aggregate interlock increased for increasing crack development. The maximum shear force was reached when the aggregate interlock stresses reached a maximum and a further increase in crack development reduced the shear force carried by the aggregate interlock. At the maximum shear force, 8% of the total shear force was carried by dowel action.

For specimen B.44.06.30.1.B with $\rho_w = 0.06\%$ (Figure 14), the shear behavior before the maximum load was similar to specimen B.44.00.00.A with aggregate interlock as the dominating shear-transfer action. The maximum shear force was reached when the aggregate interlock stresses reached a maximum. At the maximum load, 25% of the total shear force was carried by dowel action of the tensile and compressive reinforcement. Mainly because the distance between the critical shear crack and the first stirrup for the tensile reinforcement was small. After the maximum load, the contributions from aggregate interlock, residual tensile stresses, and the inclination of the compression chord almost vanished due to large crack openings and the shear contribution from the shear reinforcement and dowel action became dominant. After the maximum load, the contribution from dowel action of the tensile (and compressive) reinforcement and the shear reinforcement increased and a local maximum load was reached as the stress in the shear reinforcement reached the ultimate stress (f_u).

For specimen B.44.08.30.1.B with $\rho_w = 0.11\%$ (Figure 15), the development of the critical shear crack was similar to members with $\rho_w < \rho_{w,min}$ with a small crack development at the ultimate load. Initially, the shear force carried by aggregate interlock was dominant and gradually shifted to the shear reinforcement. At the maximum load, the aggregate interlock was still significant, while stirrups and dowel action were progressively activated and were the dominating shear-transfer action. The maximum load was reached as yielding occurred in the activated stirrups. After the maximum load, the shear behavior was similar to specimen B.44.06.30.1.B. The shear contribution from dowel was, however, less than for specimen B.44.06.30.1.B, due to a larger distance from the critical shear crack to the first intersected stirrup, with 15% at the maximum load and up to 27% after the maximum load.

For specimen B.44.08.30.2.B with $\rho_w = 0.11\%$ (Figure 16), the shear behavior was significantly different from the identical specimen B.44.08.30.1.B, mainly because the shape of the critical shear crack was flatter, which decreased the shear force carried by aggregate interlock but, on the other hand, increased the number of stirrups activated. For small crack openings, the dominating shear-transfer actions were aggregate interlock and residual tensile stresses. However, as the crack development increased, these contributions vanished and the contributions from the shear reinforcement and dowel action became dominant. At the maximum load, the crack development was severe with the shear reinforcement and dowel action as the dominating shear-transfer actions, with 23% of the total shear force carried by dowel action. After the maximum load was reached, a compressive failure occurred in the concrete in a zone located at the edge of the loading plate and towards the tip of the critical shear crack (see Figure 16). This compressive failure caused the stirrup located in this zone to detach from the concrete in the top part of the critical shear crack, after which the contribution from this stirrup vanished and dowel action from the compressive reinforcement increased. This is also reflected when comparing the load–displacement curve with the estimated sum of shear-transfer actions.

For specimen B.44.10.30.B with $\rho_w = 0.17\%$ (Figure 17), several large shear cracks developed with a distributed crack development (smeared cracking), thus reducing the crack development of the critical shear crack compared to specimens with a lower amount of

shear reinforcement. As a consequence, aggregate interlock stresses could be mobilized up to the maximum load. The maximum load was reached as a compressive failure occurred in a zone at the edge of the loading plate similar to specimen B.44.08.30.2.B (see Figure 16), causing the contribution from the stirrup in this zone and the aggregate interlock stresses to vanish. Additionally, the contribution from dowel action was almost negligible (only 4% of the total shear force). Mainly because the distance between the critical shear crack to the first stirrups was large, but also because of the less severe crack development.

For specimen B.33.06.23.B with $\rho_w = 0.11\%$ (Figure 18), the shear behavior was identical to specimen B.44.08.30.2.B. The shear force carried by dowel action from the development of the critical shear crack is shown to account for approximately 20% of the total shear force.

For specimen B.55.10.38.B with $\rho_w = 0.11\%$ (Figure 19), the shear behavior was similar to specimen B.44.08.30.2 (see Figure 16). The stirrup closest to the loading plate was, however, not activated by the critical shear crack. For this beam, approximately 38% of the total shear force is carried by dowel action, from the development of the critical shear crack and in the post peak regime. Additionally, the shear force carried by dowel action is shown to increase relative to the increase in the beam size, observed by comparing the specimen to the identical but smaller specimens B.33.06.23.B (Figure 18), B.44.08.30.1.B (Figure 15), and B.44.08.30.2.B. (Figure 16). For these beams, the distance from the critical shear crack to the first stirrup is similar. The maximum load was reached as the tensile stress in the activated stirrups reached the maximum stress (f_u) at which a compressive failure occurred in a zone at the edge of the load plate.

For specimen B.66.12.45.B with $\rho_w = 0.11\%$ (Figure 20), the shear behavior was identical to specimen B.55.10.38.B (see Figure 19). Large aggregate interlock stresses could, however, be mobilized at small crack openings for this specimen due to the steep part of the critical shear crack, causing an aggregate interlock crack to develop, after which the shear force carried by aggregate interlock was reduced. For this specimen, approximately 40% of the total shear force was carried by dowel action. The maximum load was reached as the tensile stress in the activated stirrups reached the maximum stress (f_u) at which a compressive failure occurred in a zone at the edge of the load plate.

Note that these estimates of the shear force carried by dowel action correspond to the estimates by F. Monney et al.,[53] based on strain measurements obtained by fiber-optical measurements. Furthermore, note that the plastic solution (Equation (30)) was shown to only influence the calculated shear force carried by dowel action of the reinforcement in the compression zone. Mainly because the plastic bending capacity of the compressive reinforcement was too low to activate the stirrups. For the tensile reinforcement, the plastic solution required in many cases too large deformations to be reached, and the stirrups therefore ruptured before this stage was reached.

Figure 21 shows the tested shear capacities, V_u, and the calculated shear force carried by each of the potential shear-transfer actions determined from the measured crack kinematics at V_u for the 16 analyzed specimens. In general, the sum of calculated shear contributions shows a fairly well agreement with the tested shear capacities. Here, a mean value of the ratio between the tested shear capacity and the sum of shear contributions ($V_u/\sum V_i$) of 1.02 is obtained with a coefficient of variation (COV) of 12.9%.

Figure 22 shows the calculated ratio between the individual and the sum of shear force carried by shear-transfer actions for varying the shear reinforcement ratio, ρ_w, for specimens with an effective beam depth $d = 440$ mm. From Figures 21 and 22 the following can be observed:

- For the beams without shear reinforcement, the shear force carried by dowel action is almost constant at 6%–8% of the total shear force, regardless of the beam size.

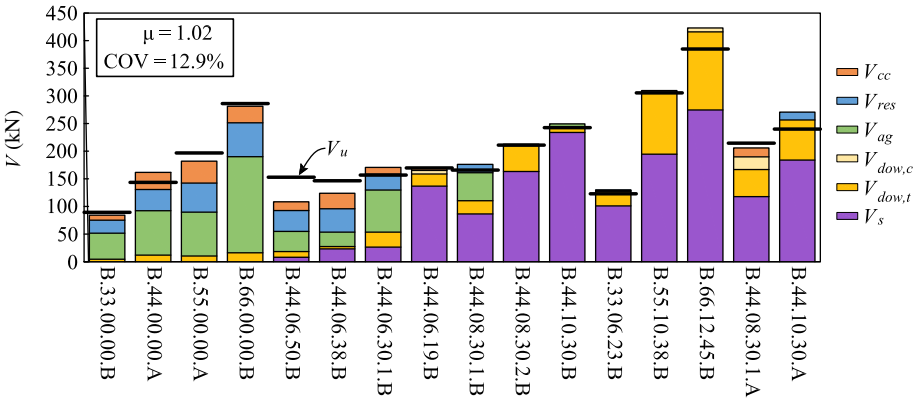

FIGURE 21 Comparison of the calculated shear force carried by each shear-transfer action at the maximum load and the experimental shear capacity, V_u.

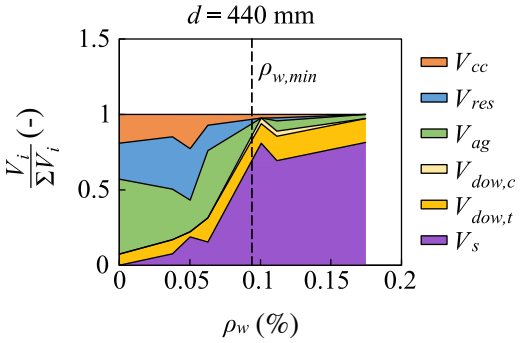

FIGURE 22 Calculated ratio between shear carried by the individual and the sum of shear-transfer actions at the maximum load for varying shear reinforcement ratio, ρ_w.

- For the beams with shear reinforcement, the shear force carried by dowel action increases relative to the beam size. For the smallest beam (B.33.06.23.B), 23% of the total shear force are carried by dowel action, whereas for the largest beam (B.66.12.45.B), 40% are carried by dowel action. This increase is mainly caused by the increase in the diameter of the longitudinal reinforcement, causing the stiffness of the longitudinal reinforcement (I_l, area moment of inertia) to increase relative to the bar diameter.
- At the minimum shear reinforcement ratio, $\rho_{w,min}$, the dominating shear-transfer actions for the shear capacity change. For specimens with $\rho_w < \rho_{w,min}$, brittle concrete contributions are dominating, that is, aggregate interlock, residual tensile stresses, and inclination of compression chord. While, for specimens with $\rho_w \geq \rho_{w,min}$, the dominating shear-transfer actions are the shear reinforcement and dowel action. Additionally, for these specimens, the shear force carried by aggregate interlock, residual tensile stresses, and inclination of the compression chord account only for 5% on average for the total shear transfer. While the shear carried by dowel action accounts for approximately 15%–20%.
- For all specimens, the contribution from dowel action of the compressive reinforcement was relatively small. Mainly because the diameter and the displacement of the compressive reinforcement were small at the maximum load.

6 | CONCLUSION

This article presents a novel dowel model to estimate the shear force carried by dowel action of both beams with and without shear reinforcement. The model was derived by assuming a linear elastic behavior for the dowel and a rigid plastic response for the shear reinforcement. Furthermore, a method to determine the dowel displacement from DIC measurements was presented. Additionally, a detailed analysis of the influence of small amounts of shear reinforcement on the shear behavior and shear force carried by each of the potential shear-transfer actions for 16 of the total 30 tested beams by Autrup et al.[8,27] is presented. The varying parameters for the investigated specimens were the shear reinforcement ratio, ρ_w, varied from 0.04% to 0.17% and the effective beam height, d, varied from 330 to 660 mm. Furthermore, identical beams without shear reinforcement were analyzed. The main conclusions of the analyses can be summarized as:

- The sum of shear force carried by each of the potential shear-transfer actions predicts fairly well the applied shear force from the development of the critical shear crack until failure. Indicating that the proposed dowel model accurately predicts the shear force carried by dowel action of the tensile and compressive reinforcement.
- For beams without shear reinforcement, only 6%–8% of the total shear force is carried by dowel action. For beams with shear reinforcement, the contribution from dowel action is significantly influenced by the distance from the critical shear crack to the first stirrup. For beams with a large distance, only 4% of the total shear force is carried by dowel action, while for the largest beam with a shorter distance, 40% of the total shear force is carried by dowel action.
- At the minimum shear reinforcement ratio, $\rho_{w,min}$, (determined according to Eurocode 2[2] and *fib* Model Code 2010[3]) the dominating shear-transfer actions for the shear capacity changes. For specimens with $\rho_w < \rho_{w,min}$, the concrete contributions are dominating, that is, aggregate interlock, residual tensile stresses, and inclination of compression chord. While for specimens with $\rho_w \geq \rho_{w,min}$, the reinforcement contributions are dominating, that is, shear reinforcement and dowel action.

The shear force carried by the brittle concrete contributions is very limited at the ultimate load for specimens with $\rho_w \geq \rho_{w,min}$.

ACKNOWLEDGMENTS

The experimental work was conducted with the help of BSc. Alexander Brandt Jensen and BSc. Jacob Henriksen during their final bachelor project. The project is financially supported by the Rambøll Foundation. The authors gratefully acknowledge these contributions.

DATA AVAILABILITY STATEMENT

The data that support the findings of this study are available from the corresponding author upon reasonable request.

ORCID

Frederik Autrup https://orcid.org/0000-0002-9344-1467
Henrik Brøner Jørgensen https://orcid.org/0000-0002-1241-8653
Miguel Fernández Ruiz https://orcid.org/0000-0001-6720-8162
Linh Cao Hoang https://orcid.org/0000-0002-5564-1599

REFERENCES

1. Muttoni A, Lurati F, Faria DV, Simões JT, Fernández Ruiz, M. Verification of existing bridges: Experiences in Switzerland on the last three decades, Italian Concrete Conference, Naples, Italy, 12–15 October 2022, 8 p.
2. Eurocode 2. Design of concrete structures—part 1–1: general rules and rules for buildings. European Committee for Standardization; 2004.
3. fib Model Code 2010. Fédération Internationale du Béton, fib Model Code for concrete structures 2010. Ernst & Sohn; 2013.
4. ACI 318-19. Building code requirements for structural concrete: commentary on building code requirements for structural concrete. Farmington Hills, Michigan: American Concrete Institute; 2019.
5. Campana S, Ruiz MF, Anastasi A, Muttoni A. Analysis of shear-transfer actions on one-way RC members based on measured cracking pattern and failure kinematics. Mag Concr Res. 2013;65(6):386–404. https://doi.org/10.1680/macr.12.00142
6. Huber P, Huber T, Kollegger J. Investigation of the shear behavior of RC beams on the basis of measured crack kinematics. Eng Struct. 2016;113:41–58. https://doi.org/10.1016/j.engstruct.2016.01.025
7. Monserrat López A, Ruiz MF, Miguel Sosa PF. The influence of transverse reinforcement and yielding of flexural reinforcement on the shear-transfer actions of RC members. Eng Struct. 2021;234:111949. https://doi.org/10.1016/j.engstruct.2021.111949
8. Autrup F, Jørgensen HB, Hoang LC. The influence of small amounts of shear reinforcement on the shear-transferring mechanisms in RC beams: an analysis based on refined experimental measurements. Struct Conc. 2022;24:1–18. https://doi.org/10.1002/suco.202200193
9. Cavagnis F, Ruiz MF, Muttoni A. Shear failures in reinforced concrete members without transverse reinforcement: an analysis of the critical shear crack development on the basis of test results. Eng Struct. 2015;103:157–73. https://doi.org/10.1016/j.engstruct.2015.09.015
10. Cavagnis F, Fernández Ruiz M, Muttoni A. An analysis of the shear-transfer actions in reinforced concrete members without transverse reinforcement based on refined experimental measurements. 2018.
11. Huber T, Huber P, Kollegger J. Influence of aggregate interlock on the shear resistance of reinforced concrete beams without stirrups. Eng Struct. 2019;186:26–42. https://doi.org/10.1016/j.engstruct.2019.01.074
12. Košćak J, Damjanović D, Bartolac M, Duvnjak I. Shear behavior of RC beams without transverse reinforcement: an analysis of crack kinematics and transfer mechanisms based on stereophotogrammetric measurements. Eng Struct. 2022;255:113886. https://doi.org/10.1016/j.engstruct.2022.113886
13. Montoya-Coronado LA, Ribas C, Ruiz-Pinilla JG, Cladera A. Time-history analysis of aggregate interlock in reinforced concrete beams without stirrups. Eng Struct. 2023;283:115912. https://doi.org/10.1016/j.engstruct.2023.115912
14. Huber T, Untermarzoner F, Kollegger J. Experimental investigation and mechanical modelling of shear failure in reinforced concrete members with plain and ribbed bent-up bars. Eng Struct. 2023;283:115793. https://doi.org/10.1016/j.engstruct.2023.115793
15. Ruiz MF, Muttoni A, Sagaseta J. Shear strength of concrete members without transverse reinforcement: a mechanical approach to consistently account for size and strain effects. 2015.
16. Yang Y, Walraven J, Uijl JD. Shear behavior of reinforced concrete beams without transverse reinforcement based on critical shear displacement. J Struct Eng. 2017;143(1):4016146. https://doi.org/10.1061/(ASCE)ST.1943-541X.0001608
17. Fisker J, Hagsten LG. Mechanical model for the shear capacity of R/C beams without stirrups: a proposal based on limit analysis. Eng Struct. 2016;115:220–31. https://doi.org/10.1016/j.engstruct.2016.02.035
18. Classen M. Shear crack propagation theory (SCPT)—the mechanical solution to the riddle of shear in RC members without shear reinforcement. Eng Struct. 2020;210:110207. https://doi.org/10.1016/j.engstruct.2020.110207
19. Autrup F, Joergensen HB. Shear capacity of RC members without shear reinforcement: a modified crack sliding model. Eng Struct. 2021;239:112147. https://doi.org/10.1016/j.engstruct.2021.112147
20. Cavagnis F. Shear in reinforced concrete without transverse reinforcement: from refined experimental measurements to mechanical models. PhD thesis. no. 8216, EPFL, Lausanne, Switzerland. 2017.
21. Tung ND, Betschoga C, Tue NV. Analysis of the crack development and shear transfer mechanisms of reinforced concrete beams with low amounts of shear reinforcement. Eng Struct. 2019;2020(222):111114. https://doi.org/10.1016/j.engstruct.2020.111114
22. Krefeld WJ, Thurston CW. Contribution of longitudinal steel to shear resistance of reinforced concrete beams. ACI J Proc. 1966;63(3):325–44. https://doi.org/10.14359/7626
23. Taylor HPJ. Shear stresses in reinforced concrete beams without shear reinforcement. Cem Concr Assoc. 1968;1–23.
24. Baumann T, Rüsch H. Versuche zum Studium der Verdübelungswirkung der Beigezugbewehrung eines Stahlbetonbalkens. Deutscher Ausschuss Für Stahlbeton 1970; Heft 210.
25. Resende TL, Cardoso CTD, Shehata CDL. Influence of steel fibers on the dowel action of RC beams without stirrups. Eng Struct. 2020;221:111044. https://doi.org/10.1016/j.engstruct.2020.111044
26. Autrup F, Jørgensen HB, Hoang LC. Dowel action of the tensile reinforcement in RC beams without shear reinforcement: novel experimental investigation and mechanical modelling. Eng Struct. 2023;279:115471. https://doi.org/10.1016/j.engstruct.2022.115471
27. Autrup F, Jørgensen HB, Hoang LC. Experimental investigation of the shear capacity of RC beams with very small amounts of shear reinforcement. Proceedings of the *fib* ymposium 2021, new trends for eco-efficiency and performance; 169:1668–1677. 2021.
28. Nielsen MP. Beton 1 del 3. Technical University of Denmark, Department of Structural Engineering. 2nd ed. 2005.

29. Gehri N, Mata-Falcón J, Kaufmann W. Automated crack detection and measurement based on digital image correlation. Construct Build Mater. 2020;256:119383. https://doi.org/10.1016/j.conbuildmat.2020.119383
30. Gehri N, Mata-Falcón J, Kaufmann W. Refined extraction of crack characteristics in large-scale concrete experiments based on digital image correlation. Eng Struct. 2022;251 (PA):113486. https://doi.org/10.1016/j.engstruct.2021.113486
31. Walraven JC. Aggregate interlock: a theoretical and experimental analysis. PhD thesis. Delft University. 1980.
32. Poli SD, Gambarova PG, Karakoç C. Aggregate interlock role in R.C. thin-webbed beams in shear. J Struct Eng. 1987;113(1):1–19. https://doi.org/10.1061/(ASCE)0733-9445(1987)113:1(1)
33. Li B, Maekawa K, Okamura H. Contact density model for stress transfer across cracks in concrete. J Fac Eng, The University of Tokyo. 1989;XL:9–52.
34. Tirassa M, Ruiz MF, Muttoni A. Influence of cracking and rough surface properties on the transfer of forces in cracked concrete. Eng Struct. 2020;225:111138. https://doi.org/10.1016/j.engstruct.2020.111138
35. Ruiz MF. The influence of the kinematics of rough surface engagement on the transfer of forces in cracked concrete. Eng Struct. 2021;231:11650. https://doi.org/10.1016/j.engstruct.2020.111650
36. Jacobsen JS, Poulsen PN, Olesen JF, Krabbenhoft K. Constitutive mixed mode model for cracks in concrete. Eng Fract Mech. 2013;99:30–47. https://doi.org/10.1016/j.engfracmech.2013.01.004
37. Ungermann J, Adam V, Classen M. Fictitious rough crack model (FRCM): a smeared crack modelling approach to account for aggregate interlock and mixed mode fracture of plain concrete. Materials. 2020;13(12):2774. https://doi.org/10.3390/ma13122774
38. Hassanzadeh M. Determination of fracture zone properties in mixed mode I and II. Eng Fract Mech. 1990;35(4–5):845–53. https://doi.org/10.1016/0013-7944(90)90169-H
39. Nooru-Muhamed MB. Mixed-mode fracture of concrete: an experimental approach. PhD thesis. Delft University of Technology. 1992.
40. Jacobsen JS, Poulsen PN, Olesen JF. Characterization of mixed mode crack opening in concrete. Mater Struct. 2012;45:107–22. https://doi.org/10.1617/s11527-011-9754-5
41. Hillerborg A, Modéer M, Petersson PE. Analysis of crack formation and crack growth in concrete by means of fracture mechanics and finite elements. Cem Concr Res. 1976;6(6):773–81. https://doi.org/10.1016/0008-8846(76)90007-7
42. Hordijk D. Tensile and tensile fatigue behaviour of concrete; experiments, modelling and analyses. Heron. 1992;37(1):1–79.
43. Tirassa M, Ruiz MF, Muttoni A. An interlocking approach for the rebar-to-concrete contact in bond. Mag Concr Res. 2021;73(8):379–93. https://doi.org/10.1680/jmacr.20.00209
44. Ruiz MF, Muttoni A, Gambarova PG. Analytical modeling of the pre- and postyield behavior of bond in reinforced concrete. J Struct Eng. 2007;133(10):1364–72. https://doi.org/10.1061/(asce)0733-9445(2007)133:10(1364)
45. Shima H, Chou LL, Okamura H. Bond characteristics in post-yield range of deformed bars. Doboku Gakkai Ronbunshu. 1987;1987(378):213–20. https://doi.org/10.2208/jscej.1987.378_213
46. Shima H, Chou LL, Okamura H. Bond-slip-strain relationship of deformed bars embedded in massive concrete. Micro and macro models for bond in reinforced concrete; 1987. https://doi.org/10.2208/jscej.1987.378_165
47. Marti P, Alvarez M, Kaufmann W, Sigrist V. Tension chord model for structural concrete. Struct Eng Int. 1998;8(4):287–98. https://doi.org/10.2749/101686698780488875
48. Cavagnis F, Ruiz MF, Muttoni A. A mechanical model for failures in shear of members without transverse reinforcement based on development of a critical shear crack. Eng Struct. 2017;2018(157):300–15. https://doi.org/10.1016/j.engstruct.2017.12.004
49. Rasmussen AB. Modelling of reinforced concrete in the serviceability limit state: a study of cracking, stiffness and deflection in flexural members. PhD thesis. Aarhus University, Department of Engineering. 2019.
50. Nielsen MP, Hoang LC. Limit analysis and concrete plasticity. 3rd ed. CRC Press; 2010. https://doi.org/10.1201/b10432
51. Sørensen JH, Hoang LC, Olesen JF, Fischer G. Testing and modeling dowel and catenary action in rebars crossing shear joints in RC. Eng Struct. 2017;145:234–45. https://doi.org/10.1016/j.engstruct.2017.05.020
52. Cantone R, Ruiz MF, Bujnak J, Muttoni A. Enhancing punching strength and deformation capacity of flat slabs. ACI Struct J. 2019;116(5):261–74. https://doi.org/10.14359/51716842
53. Monney F, Fernández Ruiz M, Muttoni A. Influence of amount of shear reinforcement and its post-yield response on the shear resistance of reinforced concrete members. Struct Concr. 2022;24:1002–34. https://doi.org/10.1002/suco.202200331

How to cite this article: Autrup F, Jørgensen HB, Ruiz MF, Hoang LC. Mechanical modeling of dowel action and the influence of small amounts of shear reinforcement on the shear-transfer actions in RC beams. Structural Concrete. 2023;24(5):5928–46. https://doi.org/10.1002/suco.202300082

APPENDIX A: SIMPLIFIED EXPRESSION FOR DOWEL ACTION

For closely spaced stirrups, the shear reinforcement can be considered to act as an equivalent evenly distributed tensile stress along the dowel ($\rho_w f_{yw}$). For an incremental dowel displacement, $\dot{\Delta}_y$, the incremental internal work dissipated in the stirrups can be estimated as:

$$\dot{W}_{I,w} = \int_0^{l_i} \rho_w \cdot f_{yw} \cdot b \cdot \dot{\Delta}_{y,w}(x) dx \quad (1)$$

where $\dot{\Delta}_{y,w}(x)$ is the incremental displacement of the evenly distributed equivalent tensile stress from the shear reinforcement. As mentioned previously, in the

deformation phase i a minimum solution is obtained if only the displacement of the ith third-order polynomial increases. The incremental displacement of the equivalent tensile stress is, therefore, determined from Equation (13) as:

$$\dot{\Delta}_{y,w}(x) = 2\frac{\dot{\Delta}_y}{l_i^3}x^3 - 3\frac{\dot{\Delta}_y}{l_i^2}x^2 + \dot{\Delta}_y \tag{2}$$

By inserting Equation (2) into Equation (1), the following solution for the incremental work dissipated in the stirrups is obtained:

$$\dot{W}_{I,w} = \frac{1}{2}\rho_w \cdot f_{yw} \cdot b \cdot l_i \cdot \dot{\Delta}_y \tag{3}$$

By establishing the work equation, that is, $\dot{W}_E = \dot{W}_{I,d} + \dot{W}_{I,w}$, in phase i the following solution for the shear transfer by dowel action is obtained:

$$V_{dow,s} = 12 \cdot E_{sl} \cdot I_l \cdot n_l \frac{\Delta_y}{l_i^3} + \frac{1}{2}\rho_w \cdot f_{yw} \cdot b \cdot l_i \tag{4}$$

Note that the contribution from the rotation (θ_A and θ_B) are not included. By minimizing Equation (4) for l_i, that is, $dV_{dow}/dl_i = 0$ and solving for l_i, the length of the dowel, l_i, in phase i can be expressed as:

$$l_i = \left(\frac{72E_{sl}I_l n_l \Delta_y}{b f_{yw} \rho_w}\right)^{1/4} \tag{5}$$

Note that this expression is more suitable as a design expression, as the influence of the distance from the critical shear crack to the first stirrup activated by dowel action is not included, which significantly influences the shear transfer by dowel action.

AUTHOR BIOGRAPHIES

Frederik Autrup, Department of Monitoring and Analyses of Existing Structures, Rambøll Denmarks A/S, Copenhagen, Denmark. Email: fau@ramboll.dk.

Henrik Brøner Jørgensen, Department of Technology and Innovation, University of Southern Denmark, Odense, Denmark. Email: hebj@iti.sdu.dk.

Miguel Fernández Ruiz, Escuela Técnica Superior de Ingenieros de Caminos, Canales y Puertos, Universidad Politécnica de Madrid, Madrid, Spain. Email: miguel.fernandezruiz@upm.es.

Linh Cao Hoang, Department of Civil and Mechanical Engineering, Technical University of Denmark, Kgs. Lyngby, Denmark. Email: linho@dtu.dk.